Available online at www.sciencedirect.com
SCIENCE DIRECT®
Journal of Molecular Catalysis A: Chemical 232 (2005) 127–134
JOURNAL OF MOLECULAR CATALYSIS A: CHEMICAL
www.elsevier.com/locate/molcata

Vanadium-metal(IV)phosphates as catalysts for the oxidative dehydrogenation of ethane

L. Lisi [a,*], G. Ruoppolo [a], M.P. Casaletto [b], P. Galli [c], M.A. Massucci [c], P. Patrono [d], F. Pinzari [d]

[a] *Istituto Ricerche sulla Combustione, CNR, P.le Tecchio, 80 Napoli, Italy*
[b] *Istituto per lo Studio dei Materiali Nanostrutturati, CNR, Via U. La Malfa, 153 Palermo, Italy*
[c] *Dipartimento di Chimica, Università degli Studi "La Sapienza", P.le A. Moro, 5 Roma, Italy*
[d] *Istituto di Metodologie Inorganiche e dei Plasmi, CNR, Monterotondo Scalo, Roma, Italy*

Received 23 July 2004; received in revised form 14 December 2004; accepted 25 January 2005

Abstract

Vanadium-exchanged Ti, Zr, and Sn-pyrophosphates have been prepared as cubic phase and tested for the oxidative dehydrogenation of ethane in the temperature range 550–700 °C in a fixed bed reactor. The catalysts have been characterised by XRD, XPS, BET surface area and TPR experiments. Vanadium exchange does not modify the cubic structure of the materials but thermal treatment under reducing or reaction conditions results in a significant loss of Sn-pyrophosphate structure, whereas Ti and Zr-pyrophosphates remain stable. All samples are active for the reaction and vanadium-Ti-pyrophosphate provides the best catalytic performances. The exchanged catalysts show a very good selectivity to ethylene, even at quite high ethane conversion, which has been attributed to the great vanadium site isolation.

Keywords: Vanadium phosphate catalyst; Vanadium oxidation state; Oxidative dehydrogenation of ethane; Ion-exchange method

1. Introduction

The oxidative dehydrogenation (ODH) of light alkanes would be a promising alternative to industrial processes for the production of olefins providing that these very reactive products are not further oxidised during the process [1].

A large number of catalysts have been proposed for the oxidative dehydrogenation of ethane [1]. Bulk and supported transition metal oxides, working at 400–500 °C through a redox cycle, give high selectivity to ethylene (40–60%) only at very low ethane conversion (20–25%), whereas basic oxides, rare earth or Li/MgO-based systems, operating at higher temperatures (600–700 °C), provide a selectivity higher than 60% at 40–60% conversion activating a hetero-homogeneous mechanism [1].

Among transition metal oxides, vanadium pentoxide has been widely investigated as bulk or supported material for the oxidative dehydrogenation of C_2–C_4 hydrocarbons, due to its high activity [2]. Furthermore, it has been reported that the addition of other elements like molybdenum, phosphorous or niobium, frequently giving rise to mixed compounds, improves catalytic performances, due to a modification of the redox properties of vanadium interacting with the other element [3].

Vanadium–phosphorous-based catalysts have been studied for both ethane and propane ODH [4–8]. More specifically, quite good selectivity but low activity have been obtained on bulk and TiO_2-supported $(VO)_2P_2O_7$ [5,6], whereas better performances have been provided for bulk or supported vanadyl *ortho*-phosphate [4,7,8]. Other metal pyrophosphates (Ce, Zr, Sn, and Ti) show catalytic activity in the ODH of *n*-butane, TiP_2O_7 giving the best performances related to its redox properties [9,10], whereas vanadium pyrophosphate is the most active but not the most selective in the

* Corresponding author. Tel.: +39 0817682261; fax: +39 0815936936.
E-mail address: lisi@irc.na.cnr.it (L. Lisi).

1381-1169/$ – see front matter © 2005 Elsevier B.V. All rights reserved.
doi:10.1016/j.molcata.2005.01.035

ODH of *iso*-butane [11]. Less attention has been paid to vanadium dispersed on metal pyrophosphate supports, notwithstanding promising results have been obtained for the oxidative dehydrogenation of ethane [12]. In principle, dispersion of vanadium in a different matrix can generate isolated active sites that are considered more selective in the partial oxidation reactions [13,14]. For this reason, in this paper the catalytic behaviour of vanadium-exchanged Ti, Zr, and Sn cubic pyrophosphates in the ethane ODH has been investigated. In fact, isolated vanadium sites are expected to be obtained by the ion-exchange method and, as a consequence, a lower oxygen lability that inhibits the total oxidation reactions.

2. Experimental

The starting materials for the preparation of the catalysts were crystalline titanium, zirconium and tin bis(monohydrogen orthophosphate) monohydrates ion-exchangers, compounds that have general formula M(IV)$(HPO_4)_2{\cdot}H_2O$ and possess a layered structure. Titanium and zirconium acid phosphates were obtained by refluxing the respective amorphous metal(IV) phosphates in 10M H_3PO_4 for 100 h [15,16]. Specifically, amorphous titanium phosphate was obtained by slowly adding, under stirring, 430 ml of 2 M HCl containing 25 g of $TiCl_4$ to 400 ml of 1.25 M H_3PO_4. After 24 h digestion, the precipitate was filtered, washed with distilled water to pH = 3–3.5 and dried over P_2O_5. The crystalline compound was obtained by refluxing the amorphous titanium phosphate in phosphoric acid in the solid/solution ratio of 1 g of solid/40 ml 10 M H_3PO_4 [15]. Amorphous zirconium phosphate was obtained by slowly adding 500 ml of 3 M HCl containing 24.4 g of $ZrOCl_2{\cdot}8H_2O$, 750 ml of a 3 M H_3PO_4 and 3 M HCl solution. As before, after digestion, filtration, washing and drying, amorphous zirconium phosphate was refluxed in phosphoric acid in the ratio of 1 g of solid/20 ml 10 M H_3PO_4 [16]. The tin-derivative was prepared by boiling a solution 1 M in $SnCl_4$, 8 M in H_3PO_4 and 4 M in HNO_3, and refluxing for 100 h since the appearance of the first nuclei of a solid material [17]. $TiCl_4$, $SnCl_4$, $ZrOCl_2{\cdot}8H_2O$, $KMnO_4$ 0.002 M standard solution and inorganic acids (H_3PO_4, H_2SO_4, HNO_3, and HCl) used for the synthesis were analytical grade Carlo Erba RPE–ACS products. $VOSO_4{\cdot}5H_2O$ (99.99% purity) was supplied by Aldrich.

The ion-exchangers will be, hereafter, denoted as H-ZrP, H-TiP, and H-SnP, respectively. When H-ZrP, H-TiP, and H-SnP were calcined at 1000 °C, the corresponding cubic pyrophosphate phases, M(IV)P_2O_7, were obtained. These latter will be denoted as M(IV)P.

The catalysts precursors were prepared by contacting H-M(IV)P ion-exchangers with solutions of vanadyl sulphate. Typically, 1 g of ion-exchanger was suspended in 350 ml 2.5×10^{-3} M $VOSO_4$ solution (initial pH = 3.6) for 2 days at room temperature. A H^+/VO^{2+} ion-exchange process occurred and, as expected, the pH of the contact solutions was more or less lowered, according to the extent of the exchange. For H-SnP the VO^{2+} uptake was evaluated by monitoring the vanadyl concentration change in the supernatant, before and after contacting, via titration with a $KMnO_4$ solution [18]. For H-ZrP, and H-TiP this method could not be used because of the low VO^{2+} uptake. In this case, it was convenient to suspend a certain amount of vanadium-exchanged precursor in a strongly acid solution (see below), in order to surely obtain a VO^{2+}/H^+ reversible process that completely releases VO^{2+} to the acid solution, and in a solid/solution ratio such that the vanadyl ions could be easily determined by $KMnO_4$ titration. Thus, 0.5 g of H-ZrP and H-TiP vanadium-exchanged materials were contacted respectively with 15 ml of 0.5 M H_2SO_4 solution for 2 h at room temperature and the VO^{2+} concentration then determined. In all cases, 5 ml of the vanadyl solutions were titrated with a 0.002 M $KMnO_4$ standard solution, using a Methrom Herisau Potentiograph model E 536 equipped with a combined Pt electrode.

The amount of vanadium exchanged by H-ZrP, H-TiP, and H-SnP was 0.10, 0.15, and 0.58%, respectively. As a consequence of the low VO^{2+} loadings, all exchanged materials showed the same TG/DTA curves and X-ray diffraction patterns as the un-exchanged H-ZrP, H-TiP, and H-SnP [15–17].

Catalysts were obtained by heating the precursors at 1000 °C for 3 h. At this temperature vanadium-containing cubic zirconium, titanium and tin pyrophosphate phases are obtained [15–17]. Taking into accounts the transformation undergone by the initial compounds, the vanadium loading in the catalysts becomes 0.11, 0.17, and 0.67% for the zirconium, titanium and tin pyrophosphate materials, respectively. The obtained catalysts will be indicated as V/ZrP, V/TiP and V/SnP.

A Philips PW 1100 diffractometer was employed for obtaining X-ray diffraction (XRD) patterns of the materials at room temperature. Ni-filtered CuKα radiation was used and the 2ϑ measurements were accurate to 0.05°.

BET surface areas of the catalysts were measured by N_2 adsorption at 77 K with a Quantachrom CHEMBET 300 instrument. Nitrogen (99.999% purity) was supplied by SOL spa (Milan). Because of the low surface area of the materials, each measurement was performed employing 300 mg of solid. Before each measurement, the catalyst was treated for 3 h at 200 °C under a He flow.

Temperature programmed reduction (TPR) was carried out using a Micromeritics TPD/TPR 2900 analyser equipped with a TCD and coupled with a Hiden HPR 20 mass spectrometer. The sample (100 mg) was reduced by a 2% H_2/Ar mixture (25 $cm^3\ min^{-1}$), heated up to 650 °C at 10 °C min^{-1} in TPR experiments. Before TPR experiments, the sample was treated in flowing air at 550 °C for 2 h.

The surface chemical composition of the samples was studied by XPS in an ultrahigh vacuum (UHV) chamber with a base pressure in the range of 10^{-8} Torr during data collection. Photoemission spectra were collected by a VG Microtech ESCA 3000 Multilab spectrometer, equipped with a standard Al Kα excitation source ($h\nu$ = 1486.6 eV) and a nine-channeltrons detection system. The binding energy (BE)

scale was calibrated by measuring C 1s peak (BE = 285.1 eV) from the surface contamination (carbon is always detected in our experimental conditions). The accuracy of the measure was ±0.1 eV. Relative concentrations of chemical elements were calculated by a standard quantification routine, including Wagner's energy dependence of attenuation length [19] and a standard set of VG Escalab sensitivity factors.

Catalytic activity tests were carried out in a fixed bed reactor operating under atmospheric pressure in the temperature range 550–700 °C. The micro-reactor consisted of a quartz tube (ϕ_e = 12.7 mm, L = 400 mm) with a porous disk (at 130 mm from the gas inlet) supporting the catalyst particles (300–400 μm). The temperature of the catalytic bed was measured using a Chromel–Alumel thermocouple located in a quartz tube (ϕ_e = 6.3 mm) co-axially put inside the reactor. In order to limit the homogeneous contribution to the ethane conversion, the reactor diameter was reduced in the post-catalytic zone (after the porous disk) and α-Al_2O_3 pellets were loaded up the catalytic bed.

The feed composition was 4% C_2H_6 and 2% O_2 in a balance of He obtained using 99.998% purity gases supplied by SON (Società Ossigeno Napoli). The contact time ranged from 0.06 to 0.4 g s N cm^{-3}. The reaction products were analysed by Hewlett–Packard series II 5890 gas-chromatograph equipped with thermal conductivity (Poraplot and Molecular Sieve column) and flame ionisation (Poraplot column) detectors for the analysis of O_2, CO, and CO_2 and for that of hydrocarbons, respectively. The concentration of O_2, CO, and CO_2 was also measured by an on-line Hartmann and Braun URAS 10 E continuous analyser. Water produced by the reaction was retained by a silica gel trap, in order to avoid condensation in the cold parts of the experimental apparatus.

The contribution of homogeneous reactions was verified by performing blank runs up to 700 °C under the same reaction conditions of catalytic tests, filling the reactor only with α-Al_2O_3 pellets. No significant ethane conversion was obtained in the blank experiments.

3. Results and discussion

3.1. BET and XRD measurements

Very low values of surface area (less than 5 m^2/g) are found for all the samples calcined at 1000 °C, as expected for cubic pyrophosphates [9].

XRD analysis performed on the same materials do not show evidence of the presence of vanadium-containing phases. Indeed, because of the low concentration of vanadium in the samples, the diffraction patterns of V/ZrP and V/TiP are coincident with those obtained for the unloaded metal(IV) pyrophosphates, as also found by Santamarìa-González et al. [12] for V/α-TiP catalysts, while in the V/SnP sample a SnO_2 phase has been evidenced by XRD data cumulated through the repetitive procedure. Fig. 1 shows the XRD patterns of

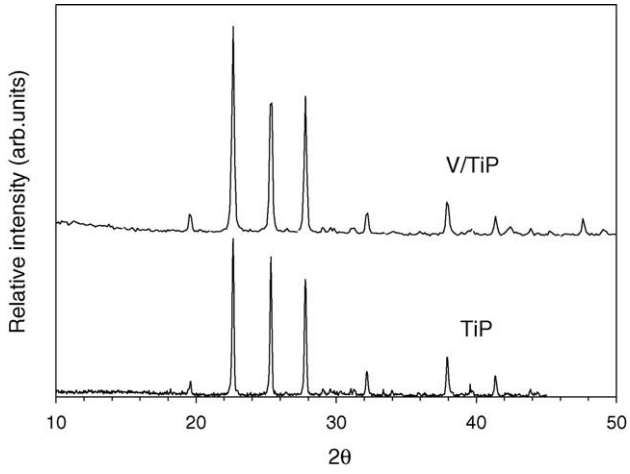

Fig. 1. X-ray diffraction patterns of TiP and V/TiP after calcination at 1000 °C.

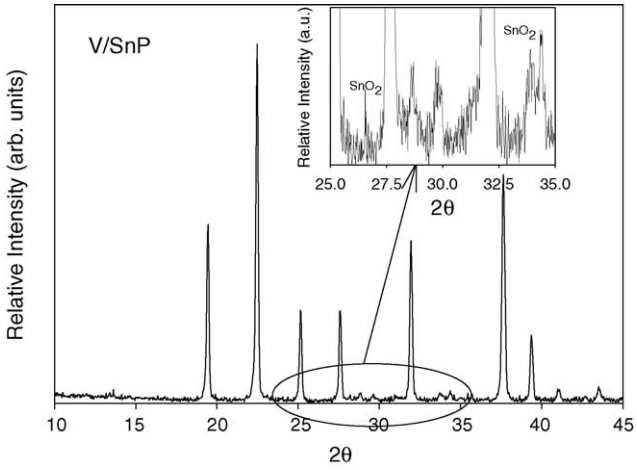

Fig. 2. X-ray diffraction pattern of V/SnP with evidenced presence of SnO_2 after calcination at 1000 °C in the inset.

TiP and V/TiP. Fig. 2 shows the presence of SnO_2 in the XRD pattern of V/SnP.

3.2. TPR measurements

The TPR profiles of the catalysts are shown in Fig. 3. In Table 1 the total hydrogen uptake (mol H_2/g of catalyst),

Table 1
Results of TPR analysis and rate of ethane consumption evaluated at 700 °C

Catalyst	H_2 uptake 10^4 (mol g^{-1})	H_2/V[a] (mol $atom^{-1}$)	$r_{C_2H_6} \times 10^6$ (mol g^{-1} s^{-1})
SnP	15.4		
V/SnP	18.5	2.4	2.2
TiP	0.41		
V/TiP	0.62	0.63	2.6
ZrP	0.19		
V/ZrP	0.24	0.23	0.4

[a] The value of H_2/V ratio has been obtained by subtracting the contribution of pure SnP, TiP, and ZrP respectively.

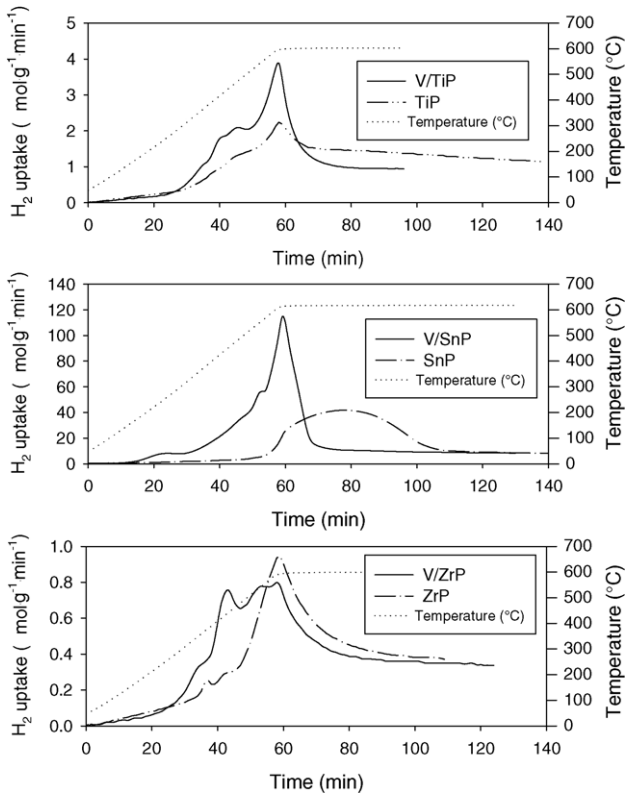

Fig. 3. TPR curves of the M(IV)P and V/M(IV)P samples.

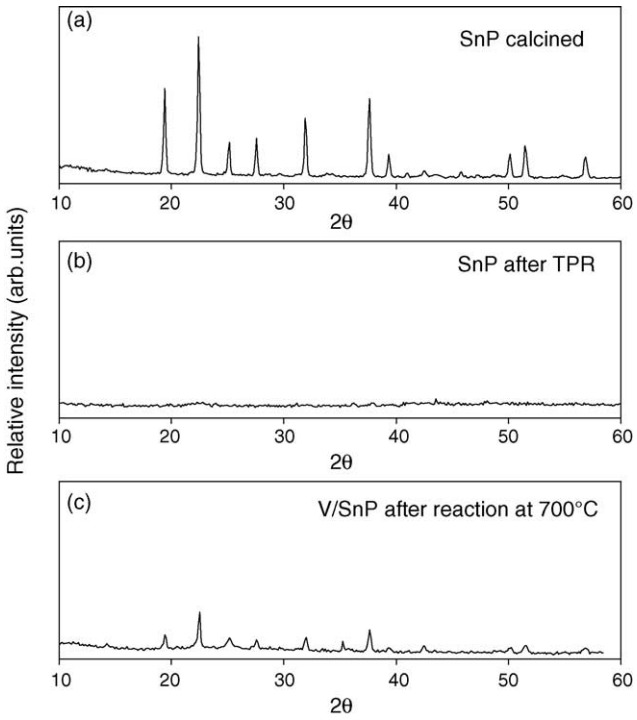

Fig. 4. XRD patterns of tin-based samples: SnP as calcined (a) and after TPR experiment (b); V/SnP sample after ODH reaction (c).

resulting from the integration of the signals, and the H_2/V ratio (mol H_2/atom V in the catalyst) are reported. For all the samples the reduction starts at quite low temperature and continues up to 650 °C. The beginning of the isothermal step inhibits further reduction of the samples.

The TPR profiles of M(IV)P are quite similar to those of the corresponding vanadium-charged materials, except for SnP which is reduced at temperatures higher than V/SnP. A limited reduction of $Sn_2P_2O_7$ up to 550 °C was also reported by Takita et al. [20] and it is in agreement with our results. The H_2 uptake of the M(IV)P materials can be associated to the partial reduction of the tetravalent metals or of phosphorous, which should lead (even if in very low extent for TiP and ZrP) to a loss of the cubic structure. The large H_2 uptake found for SnP corresponds to a 0.4 H_2/Sn ratio, which could be associated to the reduction of about half the amount of Sn^{4+} to Sn^{2+} or to the reduction of a smaller fraction of Sn^{4+} to metallic Sn^0. The latter hypothesis, qualitatively suggested by the appearance of a grey metallic deposition on the walls of the quarz cell used for TPR together with a red layer, most likely phosphorous, is validated by the XPS surface analysis of the SnP sample after the TPR experiment (see below). The XRD pattern of tin-based samples is shown in Fig. 4a. The XRD pattern of the SnP sample after TPR (Fig. 4b) shows the complete loss of crystallinity, thus suggesting that the reduction undergone is too pronounced to preserve the cubic structure.

For all samples the presence of vanadium gives rise to an increase of H_2 consumption, shown in Table 1, thus suggesting that the additional uptake can be attributed to the reduction of vanadium itself. On the base of this consideration the H_2/V ratios reported in Table 1 have been evaluated by subtracting the contribution related to the corresponding unloaded metal(IV) pyrophosphates. By supposing that vanadium is completely reduced to +3 oxidation state after the TPR experiment, a theorethical value of 0.5 for the H_2/V ratio is expected if the starting sample contained only V^{4+}. The sligthly higher value found for V/TiP could suggest that V^{4+} ions, originally introduced in the phosphate, have been partially oxidised to V^{5+}, likely during the calcination treatment. On the other hand, the very small value found for V/ZrP could be an experimental error due to the lower H_2 uptake of Zr-based samples or could indicate that not all the vanadium in the catalyst has been reduced during the TPR. Finally, the very high value obtained for V/SnP, even much higher than the stoichiometric value corresponding to the reduction $V^{5+} \rightarrow V^{3+}$, is probably an overestimated value because of the bad overlapping of TPR profiles of SnP and V/SnP. The introduction of vanadium promotes the instability of the SnP towards reduction and the loss of crystalline structure, which occurs at significantly lower temperatures.

The XRD analyses carried out on V/TiP and V/ZrP samples do not show significant differences before and after TPR experiments, thus suggesting that the possible contribution to the reduction due to other elements (Ti, Zr or P) is not sufficient to determine the complete loss of the cubic structure

Table 2
Binding energies values (BE) of the main XPS peaks and P/M(IV) atomic ratios of the samples obtained from the elemental concentrations expressed as atomic percentage (at.%)

Sample	C 1s	P 2p	O 1s	V $2p_{3/2}$[a]		Ti $2p_{3/2}$[b]		P/Ti	Zr $3d_{5/2}$	P/Zr	Sn $3d_{5/2}$[c]			P/Sn
BE (eV)	285.1	134.8	532.0	517.6	516.4	460.2	458.7		184.3		488.4	486.2	484.4	
TiP	52.1	6.6	38.2			2.8	0.4	2.1						
V/TiP	57.7	5.3	33.6	0.4	0.3	2.8		1.9						
V/TiP after ODH	44.3	7.6	43.1	0.6	0.7	3.7		2.0						
ZrP	39.5	9.4	45.8						4.9	1.9				
V/ZrP	39.5	9.1	46.8	0.3					4.4	2.1				
V/ZrP after ODH	46.0	8.2	41.6	0.2					3.9	2.1				
SnP	38.9	10.5	44.1								5.9	0.6		1.6
SnP after TPR	21.1	13.3	57.5								7.4	0.8	0.3	1.6
V/SnP	45.8	8.5	40.6	n.d.							4.6	0.5		1.7

[a] V $2p_{3/2}$ components at BE = 517.6 and 516.4 eV refer to V^{5+} and V^{4+} oxide species, respectively.
[b] Ti $2p_{3/2}$ components at BE = 460.2 and 458.7 eV are assigned to Ti phosphate and oxide species, respectively.
[c] Sn $3d_{5/2}$ components at BE = 488.4, 486.2, and 484.4 eV refer to Sn phosphate, oxide and metallic species, respectively.

and that, therefore, these two materials are more stable than the tin-derivatives under reducing atmosphere.

3.3. XPS surface analysis

XPS results of the surface characterization of the different samples are listed in Table 2. The relative chemical composition of the samples is expressed as atomic percentage (at.%).

A non-linear least-squares curve-fitting routine was used in order to separate elemental species in different oxidation states, after a Shirley background subtraction from all the XPS spectra. In all the samples, the binding energies (BE) of the main photoelectronic peaks (P 2p, Ti 2p, Zr 3d, and Sn 3d) are characteristic of elements in their normal oxidation states and detected as phosphates, in good agreement with literature data [21,22]. In all the investigated samples, O 1s spectra consist of three components, located at BE = 531.1, 532.0 and 533.1 eV, which can be assigned to (P=O–) groups; phosphates (PO_4^{3-}) and hydroxide (OH^-) species; (P–O–P) bridges groups and adsorbed water (H_2O), respectively [12,15,16]. The P 2p peak is located at BE = 134.8 eV and attributed to phosphate (PO_4^{3-}) groups. A single Zr $3d_{5/2}$ peak (FWHM = 1.8 eV) at BE = 184.3 eV is detected for all the zirconium pyrophosphate samples [20].

Evidence of metal(IV) oxide species, besides the more abundant phosphate ones, has been proved by XPS on the surface of the TiP and SnP materials. In the case of TiP, the curve-fitting of the Ti $2p_{3/2}$ peak reveals the presence of titanium oxide species at BE = 458.7 eV (13% peak area), together with the most abundant titanium phosphate species at BE = 460.2 eV (87% peak area). In the V/TiP sample, only a single Ti $2p_{3/2}$ peak is found at BE = 460.2 eV, both before and after catalysis, which is attributable to titanium phosphate species [16]. No evidence of titanium oxide was found on the surface of the vanadium-loaded TiP samples.

In the SnP and V/SnP samples, the Sn $3d_{5/2}$ peak can be fitted by two components at BE = 488.4 and 486.2 eV, which can be assigned to phosphate and oxide species, respectively [21]. This result is in agreement with the presence of a small fraction of SnO_2 detected by XRD analysis and shown in Fig. 2. The relative distribution of the different Sn species (90% phosphate and 10% oxide peak area) on the surface of the samples does not change upon vanadium loading. In the SnP sample after TPR, the Sn $3d_{5/2}$ peak fitting reveals the presence of a third component located at BE = 484.4 eV, which can be assigned to metallic Sn [21]. The surface distribution of Sn as phosphate (87% peak area), oxide (10% peak area) and metallic (3% peak area) species indicate that the reduction $Sn^{4+} \rightarrow Sn^0$ occurs at the expense of tin phosphate species, thus confirming the large H_2 uptake found for SnP (see Table 1) and the presence a red layer deposition of phosphorous on the walls of the quarz cell used for TPR.

As concerns vanadium, the highest amount of this element is detected on the surface of the V/TiP samples, as shown in Table 2. This finding allows to perform a reliable curve-fitting of the V $2p_{3/2}$ photoelectronic peak only for the V/TiP samples, both before and after the catalytic tests.

The broad V $2p_{3/2}$ peak on the V/TiP surface (FWHM $\sim$4 eV) can be decomposed by two different components located at BE = 516.4 and 517.6 eV, which can be assigned to V^{4+} and V^{5+} oxide species, respectively [21,22]. In the case of V/TiP, a great amount of V^{5+} oxide species is found on the sample surface (51% V^{5+} and 49% V^{4+} peak area), as due to the oxidising condition of calcination at 1000 °C. This result is in good agreement with the partial oxidation of V^{4+} to V^{5+} ions, already indicated by the value of the H_2/V ratio obtained in the TPR experiment and reported in Table 1.

XPS analysis of the V/TiP sample performed after catalysis still reveals the presence of both V^{4+} and V^{5+} species, but in a slightly different ratio. The relative surface distribution of vanadium species shows that the surface content of V^{4+} ions increases upon catalysis to the detriment of V^{5+} ions (47% V^{5+} and 53% V^{4+} peak area), thus confirming a progressive reduction of vanadium after the ODH catalytic runs, as al-

ready observed for vanadyl phosphates catalysts [8,22]. The simultaneous presence of V^{4+} and V^{5+} ions in these catalysts is believed to promote the selective oxidation to the olefin or to the desired oxygenated compound by the occurence of a redox mechanism [3].

As to a possible interaction of vanadium with phosphorous, it is worth noticing that vanadium oxides are the only species detected by XPS, both in the fresh and in the used catalysts. No vanadium phosphate species are found in the samples. Furthermore, a major fraction of V^{4+} oxide species is detected after the ODH test. As a consequence, the phase related to the catalytic process should be vanadium oxide interacting with the support. This finding confirms our previous results on $VOPO_4$ catalysts supported on different oxides [8,22], showing that the formation of both vanadium phosphate and vanadium oxide occurred on the surface, but that only the latter was modified after the catalytic test. The presence of a higher fraction of surface V^{4+} oxide species in the TiO_2-supported $VOPO_4$ samples resulted to be related to the good catalytic performances of the catalysts in ethane ODH, both as C_2H_6 conversion and C_2H_4 selectivity [4].

Table 2 reports the quantitative XPS results concerning the surface chemical composition of the different compounds under investigation and the surface P/M(IV) atomic ratios of all materials. For TiP and ZrP these values are very close to the stoichiometric bulk ratio of the pyrophosphate of tetravalent metals. The low P/Sn value (less than 2) is due to the surface tin hydroxide, which derives from a sensible partial hydrolysis of the surface PO_3-OH groups during the preparation of the tin-based ion-exchanger. This process always occurs when the refluxed metal(IV) acid phosphates are washed with distilled water (see experimental section) and in a very low extent for H-ZrP and H-TiP in comparison with H-SnP. Tin hydroxide transforms into tin oxide upon calcination, as found by the Sn $3d_{5/2}$ peak fitting results and by the XRD analysis (Fig. 2).

As shown in Table 2, the XPS analysis performed on V/TiP and V/ZrP samples after ODH catalytic runs reveals no significant differences in the surface quantitative composition. The surface (P/Ti) and (P/Zr) ratios remain almost the same upon catalysis. The higher vanadium content found on the V/TiP sample after catalysis is due to a lower carbon contamination of the surface in our experimental setup, which results in a higher relative content of the element. The XPS investigation of the V/SnP sample after catalytic runs was not performed, since the sample partially loses its crystalline structure, as shown in Fig. 4c.

3.4. Catalytic tests

The only products detected in the ethane ODH catalytic tests performed on the V/M(IV)P materials were C_2H_4, CO and CO_2. Oxygen conversion was always far from 100%. In order to verify the possible contribution of the pure metal(IV) pyrophosphates, the M(IV)P compounds were tested for C_2H_6 conversion under the same experimental conditions as the catalysts. A negligible activity was observed. Marcu et al. [9,10] reported a significant activity of different metal pyrophosphates in the ODH of *n*-butane, TiP_2O_7 providing the best performances. They showed that a redox cycle was activated by this catalyst, Ti^{4+} being reduced to Ti^{3+} by *n*-butane. Nevertheless, our results show that the redox ability of ethane, having more stable C–H bonds compared to the C_4 alkane, should be not sufficient to reduce metal as Ti, Zr or Sn and demonstrates that the vanadium species present on the surface of TiP, ZrP, and SnP are responsible of the significant catalytic properties acquired by the materials, thus confirming the key role of vanadium in the ethane ODH reaction.

Long run test (12 h) showed that both V/TiP and V/ZrP catalysts gave stable conversions under the experimental conditions investigated, whereas for V/SnP a slow and continuous decrease of activity was observed. No formation of $VOPO_4$, as reported by Santamaría-González et al. for a V/TiP catalyst [12], was observed for the three samples after the catalytic test, likely due to the very low vanadium content inhibiting the segregation of vanadium phosphate phases. Nevertheless, XRD analysis of V/SnP after the catalytic test (Fig. 4c) shows a significant loss of crystallinity, even if not so extreme as that observed after the TPR experiment (Fig. 4b), due to the weaker reducing power of ethane with respect to hydrogen and to the simultaneous presence of O_2 in the gas mixture. Although a catalytic role of cubic pyrophosphate structure cannot be demonstrated, it is clear that the loss of this structure results in the deactivation of vanadium active sites and, thus, that a stable structure preserves vanadium sites from modifications induced by temperature and/or reaction atmosphere.

Fig. 5 reports the ethane conversion and the selectivity towards the reaction products as a function of the W/F ratio (W: catalyst weight; F: total volumetric gas flow rate at standard conditions) at 700 °C (Fig. 5a) and as a function of the reaction temperature at a given W/F (Fig. 5b) for the V/TiP catalyst, chosen as representative.

Fig. 5a shows that the ethane conversion increases by increasing the contact time. Simultaneously, the selectivity to C_2H_4 decreases while that to CO and CO_2 increases, the latter produced in lower amount. This suggests that C_2H_4 pro-

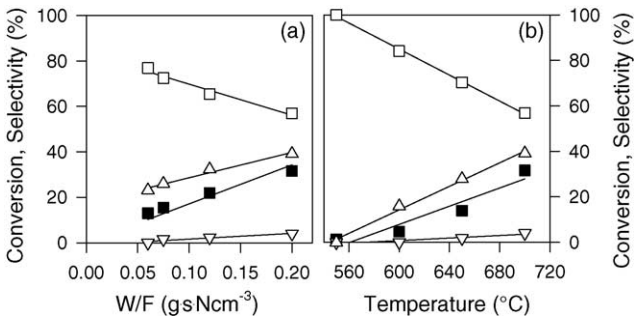

Fig. 5. C_2H_6 (■) conversion and selectivity to C_2H_4 (□), CO (△), and CO_2 (▽) as a function of W/F at 700 °C (a) and of the reaction temperature at W/F = 0.2 g s N cm^{-3} (b) for V/TiP catalyst.

duced by the C_2H_6 ODH reaction is further oxidized to CO_x at high space time, in agreement with the results previously obtained on vanadium grafted on α-titanium phosphate [12] and on bulk and supported vanadyl phosphate [3,6,7]. Fig. 5b shows that the products distribution is also very strongly affected by the temperature, since ethylene oxidation to CO_x is promoted at higher temperatures, as observed for supported vanadium oxide [23]. V/TiP shows the best catalytic activity with respect to V/ZrP and V/SnP. This could be explained as a consequence of the larger surface exposure of vanadium on V/TiP compared to V/SnP and V/ZrP, as evidenced by the XPS results (see Table 2). The reaction rate of V/TiP catalyst, evaluated under differential conditions, is slightly higher than that of V/SnP (before deactivation takes place) and much greater than that of V/ZrP, as reported in Table 1. Fig. 6 reports the ethylene selectivity obtained at different temperatures for the three different catalysts as a function of ethane conversion. As shown, the dependence of C_2H_4 selectivity on the C_2H_6 conversion is not significantly influenced by the nature of the metal(IV) pyrophosphate. From Fig. 6 it can also be inferred that, since the data connecting conversions and selectivity are all practically lying on a line having the same slope, the vanadium species on the surface of the different catalysts have probably the same nature. As a consequence, the role of pyrophosphate precursors is likely to provide exchange positions to obtain vanadium oxide centres in the final catalyst structure, which are active and selective in the ethane ODH. According to this hypothesis, the best metal phosphate is the one that has the highest number of exchange positions and the greatest thermal stability. Among the phosphates investigated, TiP is the one that better meets these requirements. We can then, conclude that the differences evidenced by Marcu et al. [9] among not-exchanged metal phosphates in the ODH of *n*-butane cannot be detected when vanadium is present. In this latter case, a higher activity compared to less reducible metal is found. Nevertheless, it cannot be completely excluded that the lattice oxygen of metal phosphates could be involved to some extent in the reaction mechanism, since these materials (with the exception of V/SnP samples) can be easily reduced without affecting the pyrophosphate structure.

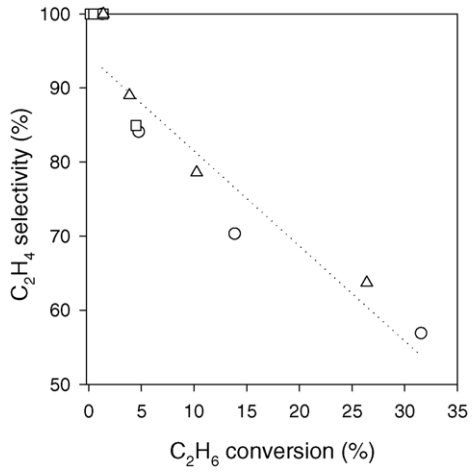

Fig. 6. Ethylene selectivity as a function of ethane conversion for V/SnP (△), V/TiP (◯), and V/ZrP (□).

Finally, it should be noticed that the isolated vanadium oxide species, deposed on the different phosphates by means of ion-exchange, show a selectivity towards ethylene significantly higher than that provided by sub mono-layer TiO_2-supported V_2O_5 [22] and sligthly higher than vanadium grafted α-TiP catalyst [12], at the same ethane conversion. Therefore, the improvement of the selectivity to C_2H_4 can be attributed to the extreme dilution of vanadium oxide species (V^{4+} and V^{5+}), which, according to the principle of site isolation [13,14], have a not easily removable oxygen, thus inhibiting the further oxidation of the ethyl intermediate to CO_x.

4. Conclusions

Vanadium-containing cubic Ti, Sn or Zr pyrophosphates are active in the oxidative dehydrogenation of ethane. XPS results indicate that vanadium is present only as oxide species and not as phosphate, both before and after the catalytic tests and that a sligth reduction of V^{5+} to V^{4+} oxide species occurs upon ODH reaction. The catalytic activity is roughly proportional to surface vanadium species, V/TiP catalyst providing the best performances due both to the good VO^{2+} exchange capacity and to the high stability under reaction conditions. V/SnP and V/ZrP catalysts show a poorer activity, related to a low stability, leading to a partial loss of the cubic structure under reaction conditions, and to a very low exchange capacity, respectively.

The extremely high vanadium dispersion obtained with the exchange method gives rise to the formation of very selective sites, consisting in isolated surface vanadium oxide species, showing a lower reducibility and, therefore, a poorer oxygen availability inhibiting the overoxidation of ethylene to carbon oxides.

References

[1] F. Cavani, F. Trifirò, Catal. Today 24 (1995) 307.
[2] E. Mamedov, V. Cortes-Corberan, Appl. Catal. A 127 (1995) 1.
[3] T. Blasco, J.M. López-Nieto, Appl. Catal. A 157 (1997) 117.
[4] P. Ciambelli, P. Galli, L. Lisi, M.A. Massucci, P. Patrono, R. Pirone, G. Ruoppolo, G. Russo, Appl. Catal. A 203 (2000) 133.
[5] L. Savary, J. Saussey, G. Costentin, M.M. Betthar, M. Gubelmann-Bonneau, J.C. Lavalley, Catal. Today 32 (1996) 57.
[6] P.M. Michalakos, M.C. Kung, I. Jahan, H.H. Kung, J. Catal. 140 (1993) 226.
[7] L. Lisi, P. Patrono, G. Ruoppolo, Catal. Lett. 72 (2001) 3.
[8] M.P. Casaletto, L. Lisi, G. Mattogno, P. Patrono, G. Ruoppolo, G. Russo, Appl. Catal. A 226 (2002) 41.
[9] I.C. Marcu, I. Sandulescu, J.M.M. Millet, Appl. Catal. A 227 (2002) 309.
[10] I.C. Marcu, I. Sandulescu, J.M.M. Millet, J. Mol. Catal. 203 (2003) 241.

[11] S.M. Al-Zaharani, N.O. Elbashir, A.E. Abasaeed, M. Abdulwahed, Catal. Lett. 69 (2000) 65.
[12] J. Santamarìa-González, M. Martìnez-Lara, M.A. Bañares, M.V. Martìnez-Huerta, E. Rodrìguez-Castellón, J.L.J. Fierro, A. Jiménez-López, J. Catal. 181 (1999) 280.
[13] R.K. Grasselli, Top. Catal. 21 (2002) 79.
[14] R.K. Grasselli, Top. Catal. 15 (2001) 93.
[15] G. Alberti, P. Cardini-Galli, U. Costantino, E. Torracca, J. Inorg. Nucl. Chem. 29 (1967) 571.
[16] A. Clearfield, J.A. Stynes, J. Inorg. Nucl. Chem. 26 (1964) 117.
[17] U. Costantino, A. Gasperoni, J. Chromatogr. 51 (1970) 289.
[18] G. Charlot, D. Bézier, Quantitative Inorganic Analysis, Methuen and Co. Ltd., London, 1957, p. 623.
[19] C.D. Wagner, L.E. Davis, W.M. Riggs, Surf. Interface Anal. 2 (1986) 5.
[20] Y. Takita, K. Sano, K. Kurosaki, N. Kawata, H. Nishiguchi, M. Ito, T. Ishihara, Appl. Catal. A 167 (1998) 49.
[21] J.F. Moulder, W.F. Stickle, P.E. Sobol, K.D. Bomben, in: J. Chastain, R.C. King Jr. (Eds.), Handbook of X-Ray Photoelectron Spectroscopy, Physics Electronics Inc., Eden Prairie, USA, 1995.
[22] M.P. Casaletto, L. Lisi, G. Mattogno, P. Patrono, G. Ruoppolo, Appl. Catal. A 267 (2004) 157.
[23] P. Ciambelli, L. Lisi, G. Ruoppolo, G. Russo, J.C. Volta, Stud. Surf. Sci. Catal. 110 (1997) 287.